Calcium Ion Fluctuations Alter Channel Gating in a Stochastic Luminal Calcium Release Site Model

Hao Ji[1], Yaohang Li[1], and Seth H. Weinberg[2(✉)]

[1] Department of Computer Science, Old Dominion University, Norfolk, VA, USA
{hji,yaohang}@cs.odu.edu
[2] Virginia Modeling, Analysis and Simulation Center (VMASC), Old Dominion University, Norfolk, VA, USA
sweinber@odu.edu

Abstract. Stochasticity and small system size effects in complex biochemical reaction networks can greatly alter transient and steady-state system properties. A common approach to modeling reaction networks, which accounts for system size, is the chemical master equation that governs the dynamics of the joint probability distribution for molecular copy number. However, calculation of the stationary distribution is often prohibitive, due to the large state-space associated with most biochemical reaction networks. Here, we analyze a network representing a luminal calcium release site model and investigate to what extent small system size effects and calcium fluctuations, driven by ion channel gating, influx and diffusion, alter steady-state ion channel properties including open probability. For a physiological ion channel gating model and number of channels, the state-space may be between approximately $10^6 - 10^8$ elements, and a novel modified block power method is used to solve the associated dominant eigenvector problem required to calculate the stationary distribution. We demonstrate that both small local cytosolic domain volume and a small number of ion channels drive calcium fluctuations that result in deviation from the corresponding model that neglects small system size effects.

Keywords: Systems biology · Chemical master equation · Fluctuation · Calcium · Ion channel · Stationary distribution · Eigenvector · Block power method

1 Introduction

In a biochemical reaction network, the copy number of the molecules in the system randomly fluctuates due to the random timing of individual reactions [1]. When the system size is small, concentration or density fluctuations are large in amplitude, and these fluctuations may alter steady-state system properties. In particular, when reactions are higher than first-order, the expected value calculated from the stationary distribution of a discrete system representation (that

R. Harrison et al. (Eds.): ISBRA 2015, LNBI 9096, pp. 162–174, 2015.
DOI: 10.1007/978-3-319-19048-8_14

accounts for fluctuations and small system size) may disagree with the steady-state value calculated from the corresponding continuous system representation (that neglects fluctuations and ignores system size effects) [2].

In many cell types, calcium (Ca^{2+}) is a key signaling molecule that drives important physiological functions, such as neurotransmitter release and myocyte contraction [3]. Ca^{2+} signaling is often localized in "spatially restricted" domains of small volume, or Ca^{2+} microdomains. Ca^{2+} influx into microdomains often occurs via Ca^{2+}-regulated Ca^{2+} channels, and the number of Ca^{2+} channels is often small. For example, in cardiomyocytes, localized Ca^{2+} signaling occurs in dyadic subspaces, estimated to contain between 10–100 Ca^{2+}-activated channels[4]. Accounting for stochasticity in Ca^{2+} channel gating, i.e., transitions between open, closed, and inactivated channel states, due to the small number of ion channels, is important and necessary to reproduce many aspects of subcellular Ca^{2+} signaling [5]. However, due to small domain volume ($0.001 - 0.1\ \mu m^3$) and resting Ca^{2+} concentration ($[Ca^{2+}]$, $0.1\ \mu M$), the expected number of Ca^{2+} ions is also typically very small ($0.06 - 6$ Ca^{2+} ions). Yet the influence of stochasticity due to Ca^{2+} ion fluctuations is not as well understood.

A common approach to modeling biochemical reaction networks that accounts for system size is the chemical master equation that governs the joint probability distribution for molecular copy number [6]. In prior work, Weinberg and Smith utilized this approach to investigate the influence of $[Ca^{2+}]$ fluctuations in minimal Ca^{2+} microdomain model, comprised of two-state Ca^{2+} channels, activated by local domain Ca^{2+} [7]. Here, we expand on this prior work to include a more physiological number of channels, channel gating model, which accounts for both Ca^{2+}-dependent activation and inactivation, and both cytosolic and luminal Ca^{2+} domains. With this increasing level of physiological detail, the associated state-space for the luminal Ca^{2+} release site model contains between $10^6 - 10^8$ elements. A novel modified block power method is used to solve the associated dominant eigenvector problem required to calculate the stationary distribution. Our paper is organized as follows: In Section 2, we briefly present the chemical master equation and calculation of the stationary distribution in a chemical reaction network. In Section 3, we describe the luminal Ca^{2+} release site model. In Section 4, we illustrate how accounting for stochasticity influences steady-state channel gating. We conclude with a brief discussion of our results in Section 5.

2 Chemical Reaction Network

2.1 Chemical Master Equation

We follow the general notation for representing a biochemical reaction network as presented in the excellent review by Goutsias and Jenkinson [6]. We describe the biochemical interactions in a system between N molecular species $X_1, X_2, \ldots, X_N$ via M reactions,

$$\sum_{n \in \mathcal{N}} \nu_{nm} X_n \rightarrow \sum_{n \in \mathcal{N}} \nu'_{nm} X_n, \quad m \in \mathcal{M}, \tag{1}$$

where $\mathcal{N} = \{1, 2, \ldots, N\}$ and $\mathcal{M} = \{1, 2, \ldots, M\}$. ν_{nm} and ν'_{nm} are the *stochiometric coefficients* that describe the number of molecules of the n-th species consumed or produced in the m-th reaction. We collect the *net stoichiometric coefficients* in the $N \times M$ matrix $\mathbb{S} = (s_{nm})$, where $s_{nm} = \nu_{nm} - \nu'_{nm}$.

In a Markov reaction network, the probability of a reaction occurring only depends on the current system state, and further, to first-order

$$\Pr\{\text{reaction } m \text{ occurs within } [t, t+dt) | \boldsymbol{X}(t) = \boldsymbol{x}\} = \pi_m(\boldsymbol{x})dt, \tag{2}$$

where vector $\boldsymbol{X}(t) = (X_1(t), X_2(t), \ldots, X_N(t))$, $\boldsymbol{x} = (x_1, x_2, \ldots, x_n)$ is a known system state, and $\pi_m(\boldsymbol{x})$ is a state-dependent function called the *propensity function*, associated with the m-th reaction. The joint probability distribution $p_{\boldsymbol{X}}(t)$ is governed by the partial differential equation, known as the *chemical master equation*,

$$\frac{\partial p_{\boldsymbol{X}}(\boldsymbol{x}; t)}{\partial t} = \sum_{m \in \mathcal{M}} \left\{ \pi_m(\boldsymbol{x} - \boldsymbol{s}_m) p_{\boldsymbol{X}}(\boldsymbol{x} - \boldsymbol{s}_m; t) - \pi_m(\boldsymbol{x}) p_{\boldsymbol{X}}(\boldsymbol{x}; t) \right\}, \tag{3}$$

where $\boldsymbol{s}_m$ is the m-th column of matrix $\mathbb{S}$.

If we index the elements in state space $\mathcal{X}$, then the master equation can be expressed as a linear system of coupled first-order differential equations

$$\frac{d\boldsymbol{p}(t)}{dt} = \boldsymbol{p}(t)\mathbb{Q}, \tag{4}$$

where $\boldsymbol{p}(t)$ is a $1 \times K$ vector containing the probabilities $p_{\boldsymbol{X}}(\boldsymbol{x}; t)$, $\boldsymbol{x} \in \mathcal{X}$, $\mathbb{Q} = (q_{ij})$ is a large $K \times K$ sparse matrix, known as the *infinitesimal generator matrix*, whose structure can be determined directly from the master equation, and K is the cardinality of (number of elements in) state space $\mathcal{X}$.

If a stationary distribution exists, then at steady-state, $\boldsymbol{p}^{ss}\mathbb{Q} = 0$, which can also be found by solution of $\boldsymbol{p}^{ss}\mathbb{P} = \boldsymbol{p}^{ss}$, where $\mathbb{P} = \mathbb{Q}\Delta t + \mathbb{I}$, $\mathbb{I}$ is the identity matrix of appropriate size, and Δt is sufficiently small that the probability of two transitions taking place in time Δt is negligible, i.e., matrix $\mathbb{P}$ is stochastic [8]. We have essentially discretized the continuous-time Markov chain into a discrete-time Markov chain with transition matrix $\mathbb{P}$. To guarantee that $\mathbb{P}$ is stochastic, $0 < \Delta t < (\max_i |q_{ii}|)^{-1}$, and specifically, for numerical considerations discussed in Stewart [8], we define $\Delta t = 0.99(\max_i |q_{ii}|)^{-1}$. The stationary joint distribution $p^{ss}_{\boldsymbol{X}}$ can be determined from $\boldsymbol{p}^{ss}$, which is calculated as described in the following section.

2.2 Numerical Calculation of Dominant Eigenvector

A Markov chain converges to a stationary distribution provided that it is aperiodic and irreducible. Let $\lambda_1, \lambda_2, \ldots, \lambda_K$ be the eigenvalues of the transition matrix $\mathbb{P}$ of the Markov chain, where $|\lambda_1| = 1 \geq |\lambda_2| \geq \ldots \geq |\lambda_K|$, and $v_1, v_2, \ldots, v_K$ are the corresponding eigenvectors. The stationary distribution of the Markov chain corresponds to the principle eigenvector v_1. Although many numerical methods

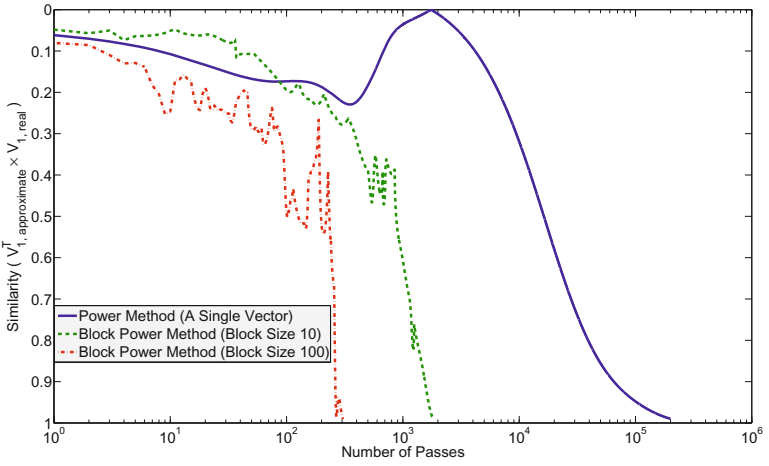

Fig. 1. Convergence of the simple power method and the block power method ($k = 10$ and 100) on a test matrix of size 1000 × 1000. The block power method significantly reduces the number of passes over the transition matrix $\mathbb{P}$ and accelerates convergence to the stationary distribution.

can be used to calculate v_1, when the transition matrix $\mathbb{P}$ is large, the power method, with a convergence rate proportional to $1/|\lambda_2|$, is typically the most feasible method with the least memory requirement.

To calculate the stationary distribution of the luminal Ca^{2+} release site model with over a million states, we develop a modified block power method. The block power method was originally designed to estimate multiple dominating eigenvalues/eigenvectors, where the convergence depends on the eigengap between the k-th and $(k+1)$-th eigenvalues, for a given block size k $(1 < k \ll K)$ [9]. Here, we are only interested in the principle eigenvector, and therefore the eigengap between $\lambda_1 = 1$ and λ_k governs the convergence speed.

Starting with a $K \times k$ orthogonal initial matrix $X^{(0)}$, the block power iteration generates the matrices sequence $\left\{X^{(i)}\right\}_{i=0}^{\infty}$ by defining

$$X^{(i)} := \mathbb{P}X^{(i-1)}, \ i = 1, 2, \ldots \tag{5}$$

For each iteration, the top-k eigenvectors of $\mathbb{P}$ are approximated by eigendecomposing a small $k \times k$ matrix ${\mathbb{B}^{(i)}}^T \mathbb{P}\mathbb{B}^{(i)}$, where $\mathbb{B}^{(i)}$ is a basis of the range space of $X^{(i)}$. More specifically, by performing block power iteration, the range space of $X^{(i)}$ becomes an approximate space capturing the dominant information of matrix $\mathbb{P}$. We construct the matrix ${\mathbb{B}^{(i)}}^T \mathbb{P}\mathbb{B}^{(i)}$ to project matrix $\mathbb{P}$ into the range space of $X^{(i)}$ and compute its eigenvectors $U^{(i)}$. Then, the top-k eigenvectors of matrix $\mathbb{P}$ can be approximated effectively through a simple matrix multiplication $\mathbb{B}^{(i)}U^{(i)}$ and the largest is selected as the approximate principle eigenvector.

Compared to the simple power method, the block power method has important advantages in handling very large transition matrices. Firstly, when the

transition matrix $\mathbb{P}$ is large, the cost of passing over $\mathbb{P}$ dominates that of other numerical computations and thus becomes the main computational bottleneck. The block algorithm can significantly reduce the number of passes over $\mathbb{P}$. Secondly, due to the fact that only the principle eigenvector is of interest, the block power method converges at a rate proportional to $1/|\lambda_k|$ instead of $1/|\lambda_2|$ as in the simple power method, which is particularly effective when the eigengap between 1 and $|\lambda_k|$ is significantly wider than that between 1 and $|\lambda_2|$. Using block sizes of $k = 10$ and 100 on a test matrix reduces the number of passes over $\mathbb{P}$ to reach convergence from on the order of 10^5 to 10^3 and 10^2, respectively (Figure 1).

3 Luminal Calcium Release Site Model

In this section, we first describe the Ca^{2+} channel gating model and Ca^{2+} domain compartmental model. We then recast the luminal Ca^{2+} release site model as a discrete biochemical reaction network, using the notation in Section 2.

3.1 Four-State Calcium Channel Gating Model

Many Ca^{2+}-regulated channels have been shown to exhibit both fast Ca^{2+} activation and slower Ca^{2+} inactivation, such as IP3 receptors [10]. The gating of Ca^{2+} channels that are activated and inactivated by local cytosolic Ca^{2+} is represented by a stochastic process with the following state transition diagram,

$$\begin{array}{ccccc} \text{(closed)} & & \mathcal{C} & \overset{k_{\mathrm{a}}^{+}c_{cyt}}{\underset{k_{\mathrm{a}}^{-}}{\rightleftharpoons}} & \mathcal{O} & & \text{(open)} \\ & k_{\mathrm{b}}^{+}c_{cyt} \Downarrow k_{\mathrm{b}}^{-} & & & k_{\mathrm{d}}^{-} \Uparrow k_{\mathrm{d}}^{+}c_{cyt} & & \\ \text{(closed, inactivated)} & & \mathcal{CI} & \overset{k_{\mathrm{c}}^{+}c_{cyt}}{\underset{k_{\mathrm{c}}^{-}}{\rightleftharpoons}} & \mathcal{I} & & \text{(inactivated)} \end{array}, \tag{6}$$

where $k_i^+ c_{cyt}$ and k_i^- are transition rates with units of time^{-1}, c_{cyt} is the local cytosolic [Ca^{2+}], and k_i^+ is an association rate constant with units of concentration^{-1}·time^{-1}, for $i \in \{a, b, c, d\}$. The channel is open when the activation site is Ca^{2+}-bound and the inactivation site is not bound (Figure 2).

In the absence of ion channel gating fluctuations, i.e., for a large number of ion channels $\mathcal{N}_c$, then the dynamics of the fraction of channels in the four states is given by the following system of ordinary differential equations,

$$\frac{df_{\mathcal{C}}}{dt} = k_{\mathrm{a}}^{-} f_{\mathcal{O}} + k_{\mathrm{b}}^{-} f_{\mathcal{CI}} - (k_{\mathrm{a}}^{+} + k_{\mathrm{b}}^{+}) c_{cyt} f_{\mathcal{C}} \tag{7a}$$

$$\frac{df_{\mathcal{CI}}}{dt} = k_{\mathrm{b}}^{+} c_{cyt} f_{\mathcal{C}} + k_{\mathrm{c}}^{-} f_{\mathcal{I}} - (k_{\mathrm{b}}^{-} + k_{\mathrm{c}}^{+} c_{cyt}) f_{\mathcal{CI}} \tag{7b}$$

$$\frac{df_{\mathcal{I}}}{dt} = k_{\mathrm{c}}^{+} c_{cyt} f_{\mathcal{CI}} + k_{\mathrm{d}}^{+} c_{cyt} f_{\mathcal{O}} - (k_{\mathrm{c}}^{-} + k_{\mathrm{d}}^{-}) f_{\mathcal{I}} \tag{7c}$$

$$\frac{df_{\mathcal{O}}}{dt} = k_{\mathrm{a}}^{+} c_{cyt} f_{\mathcal{C}} + k_{\mathrm{d}}^{-} f_{\mathcal{I}} - (k_{\mathrm{a}}^{-} + k_{\mathrm{d}}^{+} c_{cyt}) f_{\mathcal{O}}, \tag{7d}$$

where $f_{\mathcal{C}}$, $f_{\mathcal{CI}}$, $f_{\mathcal{I}}$, and $f_{\mathcal{O}}$ are the fraction of channels in states $\mathcal{C}$, $\mathcal{CI}$, $\mathcal{I}$, and $\mathcal{O}$, respectively. One of these equations is superfluous, since $f_{\mathcal{C}} + f_{\mathcal{CI}} + f_{\mathcal{I}} + f_{\mathcal{O}} = 1$.

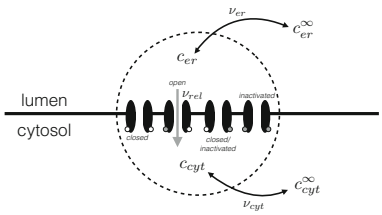

Fig. 2. Illustration of the model components and fluxes in the calcium release unit. Each Ca^{2+} channel has an activation and inactivation binding site. When only the activation site is Ca^{2+}-bound, the channel is open and Ca^{2+} is release at rate v_{rel}. Local cytosolic $[Ca^{2+}]$, c_{cyt}, relaxes to the bulk $[Ca^{2+}]$, c_{cyt}^{∞}, at rate v_{cyt}, and depleted local luminal $[Ca^{2+}]$, c_{er}, refills towards bulk luminal $[Ca^{2+}]$, c_{er}^{∞}, at rate v_{er}.

3.2 Cytosolic and Luminal Domain Compartment Model

Depletion of local Ca^{2+} near the luminal side of the Ca^{2+} channel can alter local Ca^{2+} release events, known as puffs or sparks [10]. Therefore, we consider a four compartment model that accounts for local cytosolic and luminal domains, with $[Ca^{2+}]$ of c_{cyt} and c_{er}, respectively, and bulk cytosolic and luminal compartments, with $[Ca^{2+}]$ of c_{cyt}^{∞} and c_{er}^{∞}, respectively (Figure 2). Assuming local cytosolic $[Ca^{2+}]$, c_{cyt}, relaxes to the bulk $[Ca^{2+}]$, c_{cyt}^{∞}, at rate v_{cyt}, and depleted local luminal $[Ca^{2+}]$, c_{er}, refills towards bulk luminal $[Ca^{2+}]$, c_{er}^{∞}, at rate v_{er}, and in the absence of local cytosolic domain $[Ca^{2+}]$ fluctuations, the dynamics of c_{cyt} and c_{er} are given by the following system of ordinary differential equations,

$$\frac{dc_{cyt}}{dt} = v_{rel} f_{\mathcal{O}}(c_{er} - c_{cyt}) - v_{cyt}(c_{cyt} - c_{cyt}^{\infty}) \tag{8a}$$

$$\frac{dc_{er}}{dt} = \frac{1}{\lambda}\left[-v_{rel} f_{\mathcal{O}}(c_{er} - c_{cyt}) - v_{er}(c_{er} - c_{er}^{\infty})\right], \tag{8b}$$

where v_{rel} is the luminal Ca^{2+} release flux rate, and $\lambda = \Omega_{er}/\Omega_{cyt}$ is the ratio of the local luminal and cytosolic domain volumes, Ω_{er} and Ω_{cyt}, respectively.

3.3 Stochastic Luminal Calcium Release Site Model

The stochastic luminal calcium release site model that corresponds to the channel gating and compartment models, Eqs. 7-8, respectively, and accounts for fluctuations in both channel gating and local cytosolic $[Ca^{2+}]$ can be described by the following biochemical reaction network consisting of $N = 5$ species and $M = 10$ reactions,

$$\begin{aligned} \mathcal{C} + \mathrm{Ca}^{2+}_{cyt} &\xrightarrow{\bar{k}^+_{\mathrm{a}}} \mathcal{O}, & \mathcal{O} &\xrightarrow{k^-_{\mathrm{a}}} \mathcal{C} + \mathrm{Ca}^{2+}_{cyt}, \\ \mathcal{C} + \mathrm{Ca}^{2+}_{cyt} &\xrightarrow{\bar{k}^+_{\mathrm{b}}} \mathcal{CI}, & \mathcal{CI} &\xrightarrow{k^-_{\mathrm{b}}} \mathcal{C} + \mathrm{Ca}^{2+}_{cyt}, \\ \mathcal{CI} + \mathrm{Ca}^{2+}_{cyt} &\xrightarrow{\bar{k}^+_{\mathrm{c}}} \mathcal{I}, & \mathcal{I} &\xrightarrow{k^-_{\mathrm{c}}} \mathcal{CI} + \mathrm{Ca}^{2+}_{cyt}, \\ \mathcal{O} + \mathrm{Ca}^{2+}_{cyt} &\xrightarrow{\bar{k}^+_{\mathrm{d}}} \mathcal{I}, & \mathcal{I} &\xrightarrow{k^-_{\mathrm{d}}} \mathcal{O} + \mathrm{Ca}^{2+}_{cyt}, \\ \varnothing &\xrightarrow{\alpha} \mathrm{Ca}^{2+}_{cyt}, & \mathrm{Ca}^{2+}_{cyt} &\xrightarrow{\beta} \varnothing, \end{aligned} \tag{9}$$

where reaction rates are given by $\bar{k}^+_i = k^+_i/\Omega_{cyt}$, $\alpha(\boldsymbol{x}) = \Omega_{cyt}(v_{cyt}c^{\infty}_{cyt} + v_{rel}f_{\mathcal{O}}(\boldsymbol{x})c_{er}(\boldsymbol{x}))$, and $\beta(\boldsymbol{x}) = v_{cyt} + v_{rel}f_{\mathcal{O}}(\boldsymbol{x})$. The copy numbers of channels in each state are (arbitrarily) defined as $X_1 = \mathcal{C}$, $X_2 = \mathcal{CI}$, $X_3 = \mathcal{I}$, and $X_4 = \mathcal{O}$, such that $f_{\mathcal{O}}(\boldsymbol{x}) = x_4/\mathcal{N}_c$. Similarly, the copy number of local cytosolic Ca^{2+} ions is defined as $X_5 = \mathrm{Ca}^{2+}_{cyt}$, such that $c_{cyt}(\boldsymbol{x}) = x_5/\Omega_{cyt}$. Local luminal $[\mathrm{Ca}^{2+}]$, c_{er}, is assumed to be in rapid equilibrium, such that $c_{er}(\boldsymbol{x}) = (v_{rel}f_{\mathcal{O}}(\boldsymbol{x})c_{cyt}(\boldsymbol{x}) + v_{er}c^{\infty}_{er})/(v_{rel}f_{\mathcal{O}}(\boldsymbol{x}) + v_{er})$.

The propensity functions and the net stoichiometric matrix $\mathbb{S}$ for the biochemical reaction network defined by Eq. 9 are given by

$$\begin{aligned} \pi_1(\boldsymbol{x}) &= \bar{k}^+_{\mathrm{a}}x_1x_5, & \pi_2(\boldsymbol{x}) &= k^-_{\mathrm{a}}x_4, \\ \pi_3(\boldsymbol{x}) &= \bar{k}^+_{\mathrm{b}}x_1x_5, & \pi_4(\boldsymbol{x}) &= k^-_{\mathrm{b}}x_2, \\ \pi_5(\boldsymbol{x}) &= \bar{k}^+_{\mathrm{c}}x_2x_5, & \pi_6(\boldsymbol{x}) &= k^-_{\mathrm{c}}x_3, \\ \pi_7(\boldsymbol{x}) &= \bar{k}^+_{\mathrm{d}}x_4x_5, & \pi_8(\boldsymbol{x}) &= k^-_{\mathrm{d}}x_3, \\ \pi_9(\boldsymbol{x}) &= \alpha(\boldsymbol{x}), & \pi_{10}(\boldsymbol{x}) &= \beta(\boldsymbol{x}), \end{aligned} \qquad \mathbb{S} = \begin{bmatrix} -1 & 1 & -1 & 1 & 0 & 0 & 0 & 0 & 0 & 0 \\ 0 & 0 & 1 & -1 & -1 & 1 & 0 & 0 & 0 & 0 \\ 0 & 0 & 0 & 0 & 1 & -1 & 1 & -1 & 0 & 0 \\ 1 & -1 & 0 & 0 & 0 & 0 & -1 & 1 & 0 & 0 \\ -1 & 1 & -1 & 1 & -1 & 1 & -1 & 1 & 1 & -1 \end{bmatrix}.$$

As described in Section 2, we calculate the stationary distribution and stationary statistics, given by the q-th moment of the i-th species,

$$\mu^i_q = \sum_{\boldsymbol{x}\in\mathcal{X}} x^q_i \cdot p^{ss}_{\boldsymbol{X}}(\boldsymbol{x}), \tag{10}$$

where $\mathcal{X}$ is the enumerated state-space, such that the expected channel open and inactivation probability, $\mathrm{E}[f_{\mathcal{O}}] = \mu^4_1/\mathcal{N}_c$ and $\mathrm{E}[f_{\mathcal{I}}] = \mu^3_1/\mathcal{N}_c$, respectively, and expected local cytosolic $[\mathrm{Ca}^{2+}]$, $\mathrm{E}[c_{cyt}] = \mu^5_1/\Omega_{cyt}$. We compare these stationary statistics that *account for small system size* with the corresponding steady-state values for local cytosolic $[\mathrm{Ca}^{2+}]$ and open and inactivated channel fraction that *neglect fluctuations* and *small system size effects*, c^{ss}_{cyt}, $f^{ss}_{\mathcal{O}}$, and $f^{ss}_{\mathcal{I}}$, respectively, found by the steady-state solution of Eqs. 7-8. We also calculate the *spark score*, $\mathcal{S} = \mathrm{Var}[f_{\mathcal{O}}]/\mathrm{E}[f_{\mathcal{O}}]$, an index of dispersion for $f_{\mathcal{O}}$, where the $f_{\mathcal{O}}$ variance, $\mathrm{Var}[f_{\mathcal{O}}] = [\mu^4_2 - (\mu^4_1)^2]/\mathcal{N}^2_c$, divided by the expectation $\mathrm{E}[f_{\mathcal{O}}]$, which takes values between 0 and 1. A larger spark score corresponds to more robust, spontaneous luminal Ca^{2+} release events [11].

3.4 Practical Considerations for Enumerating the State-Space

The size of the enumerated state-space $K = \mathcal{R}_5\mathcal{R}_c$, is the product of total number states for Ca^{2+}_{cyt} copy number, $\mathcal{R}_5$, and total number states for the $\mathcal{N}_c$ ion

channels, $\mathcal{R}_c$. Enumerating the state-space is straightforward when there is a natural finite range of values that each species can allow. For example, X_1, X_2, X_3 and X_4 allow values between $0, 1, \ldots, \mathcal{N}_c$. However, because Ca^{2+} influx (reaction 9) is zero-order, in theory, the local cytosolic Ca^{2+} ion maximum is infinite. In practice, we define a maximum value $\mathcal{R}_5$, for which the probability of Ca^{2+}_{cyt} exceeding such a value is negligible. We found that a reasonable value for $\mathcal{R}_5 = 2\rho$, where $\rho = \max(\lceil c_{cyt}^{max} \Omega_{cyt} \rceil, 50)$, $c_{cyt}^{max} = (v_{cyt} c_{cyt}^{\infty} + v_{rel} c_{er}^{\infty})/(v_{cyt} + v_{rel})$ is the hypothetical maximum value for c_{cyt} that occurs for a fully replete local luminal domain ($c_{er} = c_{er}^{\infty}$) and all channels open ($f_{\mathcal{O}} = 1$), and $\lceil \cdot \rceil$ is the ceiling function. Assuming channels are identical and experience the same local cytosolic $[Ca^{2+}]$, the number of distinguishable states for $\mathcal{N}_c$ channels, with $\mathcal{N}_s$ states, is given by $\mathcal{R}_c = (\mathcal{N}_c + \mathcal{N}_s - 1)!/\mathcal{N}_c!/(\mathcal{N}_s - 1)!$, where $\mathcal{N}_s = 4$ for the gating model in Eq. 6 [12]. For example, for $\Omega_{cyt} = 10^{-2}$ μm^3, $\mathcal{N}_c = 50$ channels, and standard compartment flux parameters (see Figure 3 legend), $\mathcal{R}_5 = 3012$, $\mathcal{R}_c = 23426$, and the state-space size $K \approx 7.06 \cdot 10^7$.

4 Results

We investigate the influence of small system size on the stationary properties of the luminal Ca^{2+} release site model by varying the local cytosolic domain volume Ω_{cyt} and number of Ca^{2+} channels $\mathcal{N}_c$. We plot the joint and marginal distribution for local cytosolic $[Ca^{2+}]$, c_{cyt}, and the fraction of open channels, $f_{\mathcal{O}}$, and indicate $E[f_{\mathcal{O}}]$ and $E[c_{cyt}]$ (blue circle, solid line) and $f_{\mathcal{O}}^{ss}$ and c_{cyt}^{ss} (red X, dashed line).

When the local cytosolic domain volume is small ($\Omega_{cyt} = 10^{-3}$ μm^3) and has a small number of channels ($\mathcal{N}_c = 10$), the $f_{\mathcal{O}}$-distribution is Poisson-like, while the c_{cyt}-distribution is bimodal, with one peak corresponding to a low $[Ca^{2+}]$ and zero channels open and a second peak correspond to an elevated $[Ca^{2+}]$ and a few channels open (Figure 3A). Steady-state measures, $f_{\mathcal{O}}^{ss}$ and c_{cyt}^{ss}, that neglect fluctuations correspond closely with the second peak, which illustrates that Ca^{2+} ion and gating fluctuations lead to a subpopulation of channels that are not open, which in turn reduces $E[f_{\mathcal{O}}]$ and $E[c_{cyt}]$. Further analysis of the joint distribution reveals that most of these channels are in the inactivated states, $\mathcal{I}$ and $\mathcal{CI}$ (not shown). In a local cytosolic domain of larger volume ($\Omega_{cyt} = 10^{-2}$ μm^3, Figure 3D), the two peaks in the c_{cyt}-distribution are narrower (due to smaller $[Ca^{2+}]$ fluctuations). As a consequence of smaller $[Ca^{2+}]$ fluctuations, Ca^{2+}-activation events, $\mathcal{C} \to \mathcal{O}$ and $\mathcal{CI} \to \mathcal{I}$, are less likely, and probability in the stationary distribution shifts such that the closed states, $\mathcal{C}$ and $\mathcal{CI}$, are more likely. As such, $E[f_{\mathcal{O}}]$ is reduced, and $E[c_{cyt}]$ is reduced as a consequence. However, variability in channel gating slightly increases, such that the spark score $\mathcal{S}$ increases.

As the number of channels in the domain increases ($\mathcal{N}_c = 25$, Figure 3B, E), the $f_{\mathcal{O}}$-distribution is more Gaussian-like. For a small domain volume (Figure 3B), the c_{cyt}-distribution is bimodal, as in the domain with fewer channels; however, probability has shifted primarily from the low $[Ca^{2+}]$ level to a higher $[Ca^{2+}]$

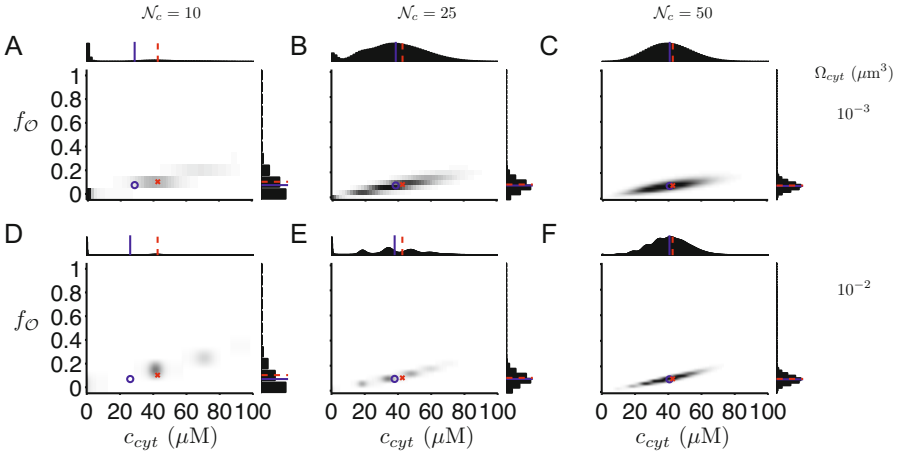

Fig. 3. Luminal Ca^{2+} release site model stationary distribution. For the parameters in each panel, the stationary joint and marginal distribution for local cytosolic $[Ca^{2+}]$, c_{cyt}, and fraction of open channels, $f_\mathcal{O}$ are shown. The expected values for $f_\mathcal{O}$ and c_{cyt}, $\mathrm{E}[f_\mathcal{O}]$ and $\mathrm{E}[c_{cyt}]$ (blue circle, solid line), respectively, and and steady-state values in the large system limit, $f_\mathcal{O}^{ss}$ and c_{cyt}^{ss} (red X, dashed line), respectively, are indicated. Parameters: $\mathcal{N}_c$ = 10 (A, D), 25 (B, E), or 50 (C, F). Ω_{cyt} = 10^{-3} (A-C) or 10^{-2} (D-F) μm^3, Channel gating [13]: $k_\mathrm{a}^+ = k_\mathrm{c}^+ = 1\ \mu\mathrm{M}^{-1}\ \mathrm{s}^{-1}$, $k_\mathrm{a}^- = k_\mathrm{c}^- = 1\ \mathrm{s}^{-1}$, $k_\mathrm{b}^+ = k_\mathrm{d}^+ = 0.01\ \mu\mathrm{M}^{-1}\ \mathrm{s}^{-1}$, $k_\mathrm{b}^- = k_\mathrm{d}^- = 0.05\ \mathrm{s}^{-1}$. Compartment fluxes and bulk concentrations [14]: $c_{cyt}^\infty = 0.1\ \mu$M, $c_{er}^\infty = 500\ \mu$M, $v_{cyt} = 10\ \mathrm{s}^{-1}$, $v_{er} = 10\ \mathrm{s}^{-1}$, $v_{rel} = 10\ \mathrm{s}^{-1}$.

level, i.e., $\mathrm{E}[c_{cyt}]$ is approaching c_{cyt}^{ss}, as expected for a larger system size. In a larger volume domain, the c_{cyt}-distribution is multimodal, with small peaks corresponding to a distinct number of open channels, including a large peak for zero open channels (Figure 3E).

As the number of ion channels increases further ($\mathcal{N}_c$ = 50), the joint distribution approaches a multivariate Gaussian distribution, with a clear positive correlation between c_{cyt} and $f_\mathcal{O}$ (Figure 3C). The expected values for $f_\mathcal{O}$ and c_{cyt}, $\mathrm{E}[f_\mathcal{O}]$ and $\mathrm{E}[c_{cyt}]$, respectively, approach the steady-state measures that neglect fluctuations, $f_\mathcal{O}^{ss}$ and c_{cyt}^{ss}, respectively. In a local cytosolic domain of larger volume, the c_{cyt}-distribution has a reduced variance, and the correlation between $f_\mathcal{O}$ and c_{cyt} is increased (Figure 3F).

In summary, over a wide range of physiological values for $\mathcal{N}_c$ and Ω_{cyt}, we can observe that as $\mathcal{N}_c$ increases, the $f_\mathcal{O}$-distribution transitions from Poisson-like to Gaussian-like, and the $f_\mathcal{O}$ variance, $\mathrm{Var}[f_\mathcal{O}]$ decreases such that the spark score $\mathcal{S}$ also decreases. For small domain volumes Ω_{cyt}, the c_{cyt}-distribution transitions from a bimodal to Gaussian distribution as $\mathcal{N}_c$ increases, whereas for a larger Ω_{cyt}, the c_{cyt}-distribution transitions from bimodal, to multimodal, to Gaussian. Over this transition, the variance of c_{cyt} initially increases and then decreases (not shown). Further, in general, $f_\mathcal{O}$ and c_{cyt} are more closely correlated for small $\mathcal{N}_c$ and larger Ω_{cyt}.

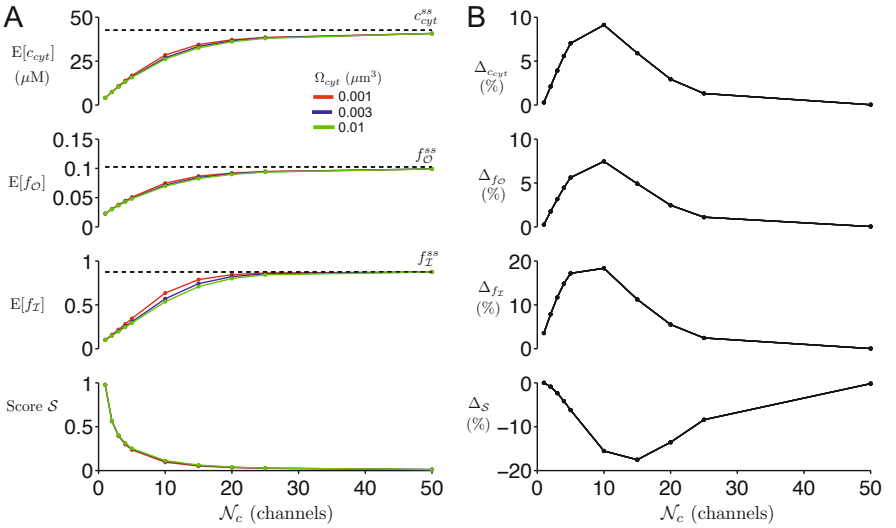

Fig. 4. Stationary statistics for the luminal Ca^{2+} release site model. (A) The expected value for local cytoslic [Ca^{2+}], and fraction of open and inactivated channels, E[c_{cyt}], E[$f_{\mathcal{O}}$], and E[$f_{\mathcal{I}}$], respectively, and spark score $\mathcal{S}$ are shown as functions of the number of channels $\mathcal{N}_c$, for different local cytosolic domain volume Ω_{cyt}. (B) The small system deviation Δ_z (Eq. 11), for $x \in \{\text{E}[c_{cyt}], \text{E}[f_{\mathcal{O}}], \text{E}[f_{\mathcal{I}}], \mathcal{S}\}$ is shown as a function of $\mathcal{N}_c$. Parameters as in Figure 3.

In Figure 4A, we plot E[c_{cyt}], E[$f_{\mathcal{O}}$], E[$f_{\mathcal{I}}$], and $\mathcal{S}$ as functions of $\mathcal{N}_c$, for different values of Ω_{cyt} (solid, colored lines). We found that $\mathcal{S}$ decreases as $\mathcal{N}_c$ increases, i.e., spontaneous sparks are less robust in domains with fewer channels. Further, E[c_{cyt}], E[$f_{\mathcal{O}}$], and E[$f_{\mathcal{I}}$] all increase as $\mathcal{N}_c$ increases and approach the steady-state values that neglects fluctuations, c^{ss}_{cyt}, $f^{ss}_{\mathcal{O}}$, and $f^{ss}_{\mathcal{I}}$, respectively (black, dashed). We found that for small number of channels, $\mathcal{N}_c$ near $10-20$, there is a noticeable difference between these metrics as the cytosolic domain volume increases from $\Omega_{cyt} = 10^{-3}$ (red) to 10^{-2} μm^3 (green). We quantified this deviation, referred to as the small system size deviation in [7],

$$\Delta_z = \frac{\text{E}[z] - \text{E}[z]_\infty}{\text{E}[z]_\infty}, \tag{11}$$

where z is the measurement for the smallest domain volume ($\Omega_{cyt} = 10^{-3}$ μm^3), E[z]$_\infty$ is the measurement for the largest domain volume ($\Omega_{cyt} = 10^{-2}$ μm^3), and $z \in \{c_{cyt}, f_{\mathcal{O}}, f_{\mathcal{I}}, \mathcal{S}\}$. Δ_z for the four measurements are biphasic functions of $\mathcal{N}_c$ (Figure 4B). For $z \in \{c_{cyt}, f_{\mathcal{O}}, f_{\mathcal{I}}\}$, $\Delta_z > 0$ (positive) and is maximal at $\mathcal{N}_c = 10$, i.e., E[c_{cyt}], E[$f_{\mathcal{O}}$], and E[$f_{\mathcal{I}}$] all decrease as local cytosolic domain volume Ω_{cyt} increases. $\Delta_{\mathcal{S}} < 0$ (negative) and is minimal at $\mathcal{N}_c = 15$, i.e., $\mathcal{S}$ increases as Ω_{cyt} increases. The small system size deviation is largest in magnitude for $f_{\mathcal{I}}$.

5 Conclusions

Small system size effects are known to influence dynamics in many settings, including biochemical, epidemiological, social, and neural networks [6]. Fluctuations in Ca^{2+} microdomain signaling due to stochastic gating of ion channels are well-known [5]; however, fewer studies have also accounted for influence of fluctuations in $[Ca^{2+}]$ due to small microdomain volume [7, 15, 16].

In this study, we sought to determine the role of fluctuations in Ca^{2+} channel and ion fluctuations in influencing steady-state properties of a luminal Ca^{2+} release site model. The state-space for the discrete model is very large, on the order of $10^6 - 10^8$ elements, for a physiological number of channels, channel gating model, and domain volume, and a novel method was utilized to solve the corresponding eigenvector problem. We demonstrate that small system size effects, due to both the small number of channels $\mathcal{N}_c$ and local cytosolic domain volume Ω_{cyt}, influence stationary statistics for the system, including open channel probability and spark score. Further, we are able to identify properties of local cytosolic domains, i.e., parameter values for $\mathcal{N}_c$ and Ω_{cyt}, for which stationary characteristics, such as channel open probability and local $[Ca^{2+}]$ levels, do not agree with the corresponding model that neglect small system size effects. Expected values for c_{cyt}, $f_{\mathcal{O}}$, $f_{\mathcal{I}}$, and $\mathcal{S}$ were found to have a strong dependence on the number of channels in the domain, $\mathcal{N}_c$. Further, for a given number of channels, in particular, small values near 10-15, these measures deviated as Ω_{cyt} increases, demonstrating that fluctuations in Ca^{2+} ions, in addition to channel gating, also influence system stationary properties. Since local domain, spontaneous Ca^{2+} release events can greatly influence global Ca^{2+} signaling and homeostasis [11, 14], our work suggests that predictive whole-cell models of Ca^{2+} signaling should account for Ca^{2+} ion fluctuations and small system size effects.

In this study, we consider a Ca^{2+} channel gating model that accounts for both Ca^{2+}-dependent activation and inactivation and a Ca^{2+} compartmental model that includes first-order passive exchange between local and bulk domains [10]. Interestingly, we found that small system deviations, $\Delta_{c_{cyt}}$ and $\Delta_{f_{\mathcal{O}}}$, are positive, in contrast with our prior work analyzing a minimal domain and gating model [7], demonstrating that accounting for more physiologically-detailed models of domain compartments and gating is important. In pathological settings, the kinetics of these processes may be altered, leading to more frequent spontaneous Ca^{2+} release events. Further, luminal Ca^{2+} channel gating dynamics may be more complex, including multiple closed, inactivated, and refractory states. Further studies are needed to investigate the influence of small system effects in these settings. However, the general approach presented is independent of model parameters, compartments, or the channel gating model. The stationary statistics of the expansive state-space associated with a pathological or expanded gating model can be similarly analyzed.

Acknowledgments. The authors acknowledge and thank Old Dominion University High Performance Computing for use of the Turing cluster to perform numerical calculations. This work is partially supported by NSF grant 1066471 (YL) and by an ODU Modeling and Simulation Fellowship (HJ). This work used the Extreme Science and Engineering Discovery Environment (XSEDE), which is supported by NSF grant ACI-1053575.

References

1. Keizer, J.: Statistical Thermodynamics of Nonequilibrium Processes. Springer Science & Business Media (August 1987)
2. McQuarrie, D.A.: Kinetics of small systems. I. J. Chem. Phys. 38(2), 433–436 (1963)
3. Berridge, M.J.: Calcium microdomains: organization and function. Cell Calcium 40(5-6), 405–412 (2006)
4. Franzini-Armstrong, C.: Architecture and regulation of the Ca2+ delivery system in muscle cells. Appl. Physiol. Nutr. Metab. 34(3), 323–327 (2009)
5. Greenstein, J.L., Winslow, R.L.: An integrative model of the cardiac ventricular myocyte incorporating local control of Ca2+ release. Biophys. J. 83(6), 2918–2945 (2002)
6. Goutsias, J., Jenkinson, G.: Markovian dynamics on complex reaction networks. Physics Reports 529(2), 199–264 (2013)
7. Weinberg, S.H., Smith, G.D.: Discrete-State Stochastic Models of Calcium-Regulated Calcium Influx and Subspace Dynamics Are Not Well-Approximated by ODEs That Neglect Concentration Fluctuations. Computational and Mathematical Methods in Medicine 2012(12), 1–17 (2012)
8. Stewart, W.J.: Introduction to the Numerical Solution of Markov Chains. Princeton University Press (1994)
9. Golub, G.H., Van Loan, C.F.: Matrix Computations. JHU Press (December 2012)
10. Huertas, M.A., Smith, G.D.: The dynamics of luminal depletion and the stochastic gating of Ca2+-activated Ca2+ channels and release sites. Journal Theor. Biol. 246(2), 332–354 (2007)
11. Wang, X., Weinberg, S.H., Hao, Y., Smith, G.D.: Calcium homeostasis in a local/global whole cell model of permeabilized ventricular myocytes with a Langevin description of stochastic calcium release. Am. J. Physiol. Heart Circ. Phsyiol., 1–62 (November 2014)
12. Deremigio, H., Lamar, M.D., Kemper, P., Smith, G.D.: Markov chain models of coupled calcium channels: Kronecker representations and iterative solution methods. Phys. Biol. 5(3), 036003 (2008)
13. Mazzag, B., Tignanelli, C.J., Smith, G.D.: The effect of residual Ca2+ on the stochastic gating of Ca2+-regulated Ca2+ channel models.. Journal of Theoretical Biology 235(1), 121–150 (2005)
14. Hartman, J.M., Sobie, E.A., Smith, G.D.: Spontaneous Ca2+ sparks and Ca2+ homeostasis in a minimal model of permeabilized ventricular myocytes. Am. J. Physiol. Heart Circ. Physiol. 299(6), H1996–H2008 (2010)

15. Koh, X., Srinivasan, B., Ching, H.S., Levchenko, A.: A 3D Monte Carlo Analysis of the Role of Dyadic Space Geometry in Spark Generation. Biophys. J. 90(6), 1999–2014 (2006)
16. Weinberg, S.H., Smith, G.D.: The Influence of Ca2+ Buffers on Free [Ca2+] Fluctuations and the Effective Volume of Ca2+ Microdomains. Biophys. J. 106(12), 2693–2709 (2014)